

# Plasmons Coupling and Anti-Crossing of Nanometal Asymmetric Dimer

Jianxin Zhang

Shaanxi Normal University

Jian Zhang

Shaanxi Normal University

Yongfang Li (✉ [yfli@snnu.edu.cn](mailto:yfli@snnu.edu.cn))

Shaanxi Normal University <https://orcid.org/0000-0002-4472-5594>

---

Original Article

Keywords:

Posted Date: February 8th, 2021

DOI: <https://doi.org/10.21203/rs.3.rs-162249/v1>

License: © ⓘ This work is licensed under a Creative Commons Attribution 4.0 International License.

[Read Full License](#)

---

# **Plasmons coupling and anti-crossing of nanometal asymmetric dimer**

Jianxin Zhang, Jian Zhang, Yongfang Li\*

*School of Physics and Information Technology, Shaanxi Normal University, Xi'an 710119, China*

\*yfli@snnu.edu.cn

## **Abstract**

In this paper, by defining a new physical quantity called as the frequency offset in the harmonic oscillator model and combining with the established plasmon coupling model, we successfully explain the anti-crossing property caused by plasmon coupling of dimer composed of a silver nanoring and a silver nanorod. In the plasmons coupling model, we reasonably reveal that the physical mechanism of the coupling between bright mode and dark mode of the plasmons is mainly represented by the coulomb potential and the electrostatic potential. With this model, we explain also the asymmetric feature the variation of frequency offset and coupling coefficient with coupling distance.

**Keywords** Anti-crossing • Frequency offset • Coulomb potential and electrostatic potential • Harmonic oscillator model

## **1. Introduction**

The surface plasmons resonance generated by light field excitation of metal nanostructures is sensitive to the shape, size, structure, material and surrounding environment. The interaction between plasmons of the multiple nanostructures generates some phenomenons such as electromagnetically induced transparency (EIT)[1-18], Fano, crossing, and anti-crossing modes caused by the split of resonant modes, etc. These phenomenons have closely linked the coupling

of plasmonic , and the coupling model of harmonic oscillators is the primary one of the research method to study plasmons coupling. For example, Zhang et al. and Alzar et al. studied the like-EIT effect in trimetric plasmons with the coupling model of a harmonic oscillator[16, 18]. L. Novotny explored the splitting of energy states of atoms and light fields in a strongly coupling process in quantum physics using a harmonic oscillator coupling model[19]. L. Andrea et al. theoretically and experimentally demonstrated that a simple oscillator model is provided to predict and fit the plasmonic far-field scattering[20]. H. Cheng et al. analytically described destructive interference for the tunable plasmonically induced transparency (PIT) with the coupling Lorentz oscillator model[21]. Aiming at the coupling asynchrony of plasmons related to the coupling phase, we introduce a phase factor into the coupling coefficient in the coupling model of the harmonic oscillator, and reveal the mechanism of the asymmetry of the absorption spectrum after coupling[22, 23]. Z. Jorge et al. investigated the maximum near-field enhancements for the localized plasmons of metallic nanoparticles and nanostructures[24]. The results came directly from the physics of a driven and damped harmonic oscillator. J. B. Lassiter et al. explained the Fano resonance of nanodisk clusters visually by using a coupling oscillator picture[25]. Coupling oscillator is an intuitively and commonly physical model which interprets EIT, energy level repulsion, non-adiabatic process, and fast adiabatic passage et.al.

Except for the coupling oscillator model, T. J. Davis and D. E. Gómez proposed a simple algebraic approach for modeling localized surface plasmons[26], which is derived from an electrostatic formalism and appropriate for near-field interaction of localized surface plasmons.

In this paper, the plasmons coupling characteristics of asymmetric dimers composed of a silver nanoring and a silver nanorod are studied by changing the structure parameters with the Finite element method (FEM). The results show that the bright mode of the metal nanoring splits into two modes under the influence of the dark mode of metal nanorods, which show an asymmetric anti-crossing feature with the change of the nanorod's length. The two splitting modes have asymmetric evolution characteristics when the gap between the naorod and nanoring is changed. When the dimer is rotated and form different angles between the nanorod and the linearly polarized light, the bright and dark mode of the naorod are generated at the meantime in the

polarized light field excitation. The influence of the bright mode on the nanoring is smaller than that of the dark mode. In order to give a clear physical explanation of the numerical results, we introduce a new coupling physical quantity  $\Delta\Omega$  in the coupling model of a harmonic oscillator. By using the plasmonic coupling (CPEP) model[28, 29], the physical mechanism of the asymmetric anti-crossing feature is revealed, it represents the Coulomb potential as the dominant potential and the electrostatic potential as the supplementary. The results obtained from this model agree well with the numerical calculation.

## 2.Dimer structure design

We design a dimer structure consisting of a metal nanoring and a metal nanorod to be arranged periodically in an  $x$ - $y$  plane on the glass substrate, as shown in Fig. 1(a, b). The length, width and the thickness of the one unit are  $a = 400$  nm,  $b = 400$ nm and 100 nm in Fig. 1(a), respectively. As shown in Fig. 1(b), the thickness and the width of the nanorod both are 20 nm, the outer radius length and the inner radius length of the nanoring are 50 nm and 40 nm, respectively, and the thickness is 20 nm. The length of the nanorod is noted as  $h$ , and the gap between the nanorod and the nanoring is labeled as  $g$ ; dissipation factor of the glass substrate is 0.0001.

The Finite element method (FEM) was used to study the absorption characteristics, electric field, and charge distribution of dimer structure under the action of the light field; the material of dimer is silver, which is more sensitive to the light field and has wider spectral absorption. The dielectric constant of silver has been provided by the literature[27]. The perfectly matched layers which are used to ensure perfect absorption and reduce scattering should be set up in numerical simulation. The incident direction of the light field is along the  $z$ -axis, and the linear polarization direction of the light field is along the  $x$ -axis.

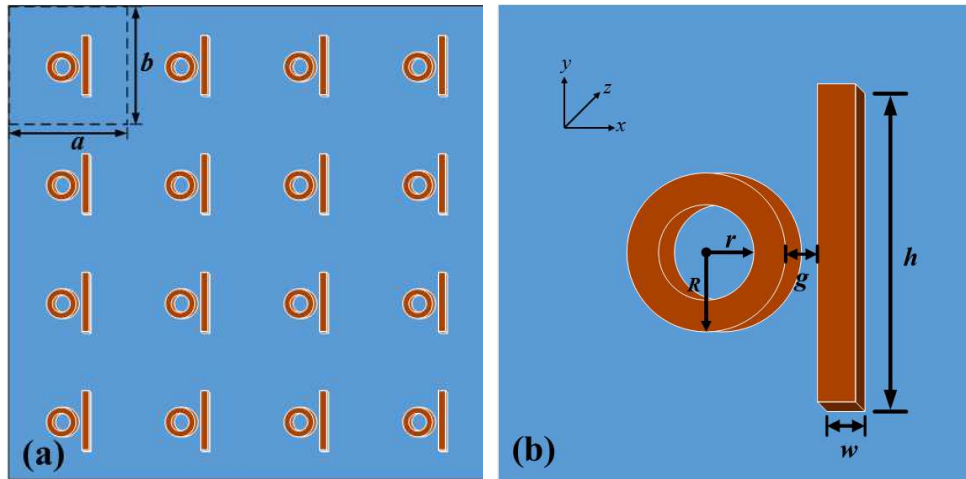


**Fig. 1** Schematic diagram of the nanoring-nanorod dimer structure. **(a)** Periodically arranged dimer units. **(b)** Specific structure of a dimer unit.

### 3. The coupling characteristics of Nanoring and Nanorod

The Fig. 2 shows the evolution of the two resonance absorption spectra of the nanorings with the increase of the nanorod's length in the dimer. The first line at the front in the Fig. 2, which the length of the nanorod is 110 nm, has only one the absorption peak, and it is resonant mode of the nanoring. The characteristic of the absorption spectra of the Fig. 2 appears that the intensity of the one absorption peak is from weak gradually to stronger, and another is from stronger gradually to weak. At the same time, both the short-wavelength and the long-wavelength resonance modes of the nanoring move total to the long-wavelength region, but the two modes move in different patterns. Both absorption peaks exhibit anti-cross characteristics with the increase of the nanorod's length. The two modes are closest when the nanorod length is 250 nm.

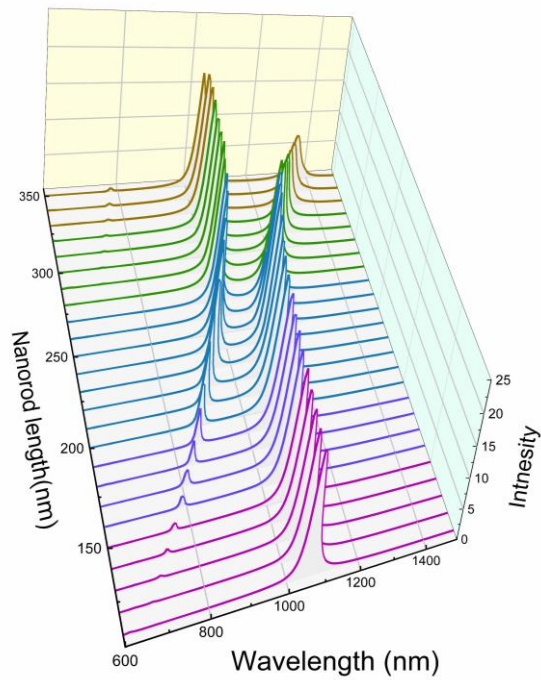


**Fig. 2** The evolution of the two resonant absorption spectra of the nanoring with the length of the nanorods in the dimer. This is an anti-crossing characteristic. The distance between the two is kept at  $g = 20$  nm.

When the polarized direction of the light field is perpendicular to the nanorod, the nanoring is excited only by the light field and the plasmons are produced on the surface of the nanoring. However, the plasmons of the nanorods are induced by the plasmons of the nanoring, rather than the result of direct excitation of the light field. Therefore, the increase of the nanorod's length will change the distribution of the surface charge of the nanorod and the oscillation frequency of the plasmon, but does not affect the amount of total charges of the nanorod. In a word, the change of the surface charge distribution of the nanorod will lead to the change of the electric field of the nanorod and affect the coupling between the plasmons. This result will give a reasonable explanation in the coupling model established later.

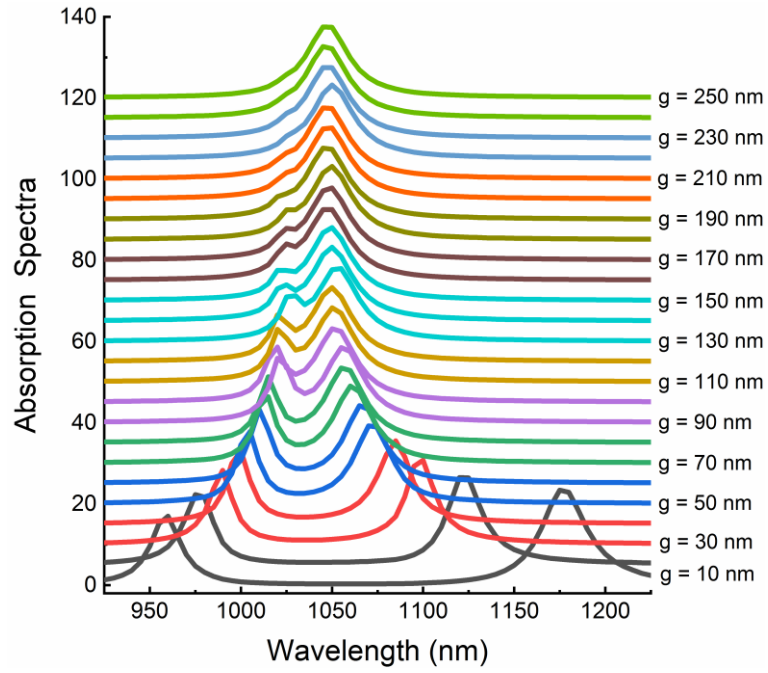


**Fig. 3** The evolution of the two resonant absorption spectra of nanorings with the change of the gaps between nanorod and nanoring in the dimer. The length of the nanorod is  $L = 250$  nm.

Fig. 3 shows the evolution of two split modes with the change of the gap between nanoring and nanorod. The closer the gap are, the stronger the coupling and the larger the frequency different of the splitting mode. As the gap increases, the coupling strength will weaken; at the same time, the two modes exhibit an asymmetry evolution law. When the gaps is  $g = 70-90$  nm, the absorption spectra shows an EIT-like effect. When the gap is greater than 200 nm, only a single resonant absorption mode of the nanoring appears, which indicates that the coupling is weak.

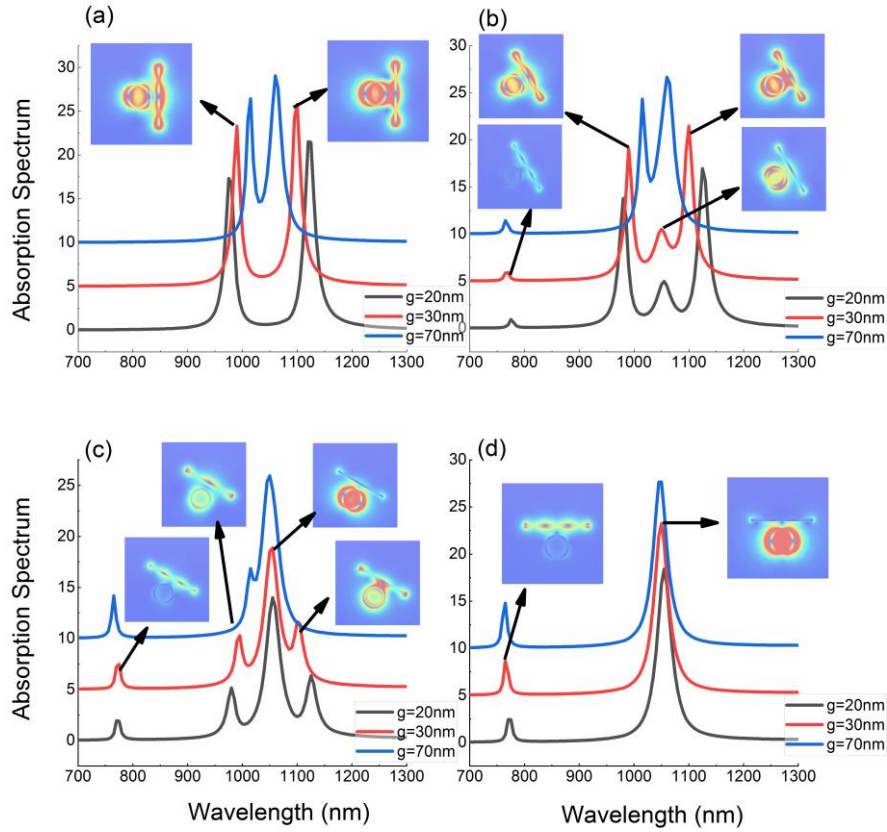


**Fig. 4** The evolution of the absorption spectra with the change of the angles between the polarization direction of the excitation light and the nanorod, which are  $90^\circ$ ,  $60^\circ$ ,  $30^\circ$ , and  $0^\circ$ , respectively.

When the polarization direction of the excited light field is perpendicular to the silver nanorods, that is,  $90^\circ$ , the nanorods cannot be excited by the light field and only be induced by the nanoring to generate plasmons in the longitudinal direction. Then, the coupling between the bright mode of the nanoring and the dark mode of the nanorod splits the bright mode into two modes, the electric field distribution is shown in Fig. 4(a). When the angle between the polarization direction of the light field and the nanorod is  $60^\circ$ , a new absorption peak in the absorption spectra appears in the short-wave region, which is dominated by the electric field of the nanorod. At the same time, there is also a smaller absorption peak between the two splitting absorption peaks, which is dominated by the nanoring electric field, as shown in Fig. 4(b). This is because the polarized light field can be decomposed into components of the vertical nanorods and parallel nanorods, the parallel component of the light field excites the nanorods and produces a short-wavelength resonant absorption peak, and vertical component of the light field excites the nanoring and produces an intermediate resonant absorption peak between splitting modes. When the angle

between the polarization direction of the light field and the nanorod is  $30^\circ$ , the polarized light intensity of the parallel nanorod component increases, so that the two newly-appearing absorption peaks increase as well, as shown in Fig. 4(c). Due to the decrease of the vertical component of the light field, the two absorption peaks of splitting are obviously weakened. When the angle between the polarization direction of the light field and the nanorod is  $0^\circ$ , it means that the polarized light has only the component of the parallel nanorod. The short wavelength absorption peak comes from the nanorod excited by the light field, and the other comes from the nanoring excited by the light field, as shown in Fig. 4(d).

The above numerical calculation results show that the coupling process between the plasmons mainly occurs between the bright mode of the nanoring and the dark mode of the nanorod, meanwhile, the intensity of the coupling is related to the structure, as shown in Fig. 2, Fig. 3 and Fig. 4(b, c, d). The change of the nanorod's length can cause anti-crossing characteristics of the absorption peaks; the bright mode splitting process of the nanoring can be shown by changing the gap between the nanoring and the nanorod, and the two absorption peaks exhibit asymmetric evolution with gap variation. In order to explain the above numerical calculation results, we introduce a new coupling physical quantity  $\Delta\Omega$  and establish a plasmonic coupling (CPEP) model[28, 29]. The physical mechanism of the asymmetric anti-crossing feature is revealed by the new model, and the calculation results with the model are agreed well with the numerical calculation.

#### 4. Coupling model

##### (1) Coupling model of the classical oscillator

In the following discussion, we suppose that the bright and dark mode can be considered as two harmonic oscillators with same mass, the resonant frequencies of the two oscillators are  $\omega_A$  and  $\omega_B$ , respectively, and the coupled coefficient is  $\kappa$ . The bright mode is expressed as  $a(\omega)e^{i\omega t}$ , which is excited by the incident light field ( $E = E_0 e^{i\omega t}$ ); the dark mode can be written as  $b(\omega)e^{i\omega t}$ , which cannot be directly excited by the incident light field. A new parameter is defined, i.e. the frequency offset  $\Delta\Omega$  produced from the coupling of two harmonic oscillators. The resonant

frequency ( $\omega_A$ ) of one oscillation convert to a new frequency  $\omega_A'$ , in which  $\omega_A' - \omega_A = \Delta\Omega$ ; at the same time, one of another is expressed as  $\omega_B = \omega_A + \Delta\Omega - \Delta\omega$ ,  $\Delta\omega$  is the difference between  $\omega_A$  and  $\omega_B$  and is so small that  $\Delta\omega = \omega_{A,B}$ . When the coupling between the two oscillators disappears, the frequency offset disappears at the same time, that is,  $\kappa = \Delta\Omega = 0$ .  $\delta = \omega_A - \omega$  is the difference of frequency between the acting light field and the resonant frequency of the oscillator. According to the previous description, the coupling equation of bright mode and dark mode can be written as[16, 28, 29]

$$\begin{pmatrix} \delta + \Delta\Omega & \kappa \\ \kappa & \delta + \Delta\Omega - \Delta\omega \end{pmatrix} \begin{pmatrix} a \\ b \end{pmatrix} = \begin{pmatrix} E_0 \\ 0 \end{pmatrix} \quad (1)$$

If only considering case of the resonant excitation, it means is that the frequency of the light field is equal to  $\omega_A$  ( $\delta = \omega - \omega_A = 0$ ), then the eigenfrequencies of the coupled oscillators can be written as

$$\begin{pmatrix} \omega_1 \\ \omega_2 \end{pmatrix} = \begin{pmatrix} \Delta\Omega - \frac{\Delta\omega}{2} - \sqrt{\kappa^2 + \left(\frac{\Delta\omega}{2}\right)^2} \\ \Delta\Omega - \frac{\Delta\omega}{2} + \sqrt{\kappa^2 + \left(\frac{\Delta\omega}{2}\right)^2} \end{pmatrix} \quad (2)$$

Fig. 5 shows the evolution of the eigenfrequency of the coupled oscillators obtained from the coupled oscillator model. Obviously, when the coupling exists, the eigenvalues show an anti-crossing and symmetrical evolution law with the resonant frequency difference of the two oscillators. The result of the Fig. 5(b) is somewhat similar to the result of Fig. 2, and the difference is that the result of the Fig. 2 exhibit asymmetrical anti-crossing characteristics. This shows that the results of numerical calculations are not determined by a single variable or a single physical quantity. In the case  $\Delta\Omega \neq 0$ , the evolution pattern is the same as that in Fig. 5(b) except that the two curves shift upward.

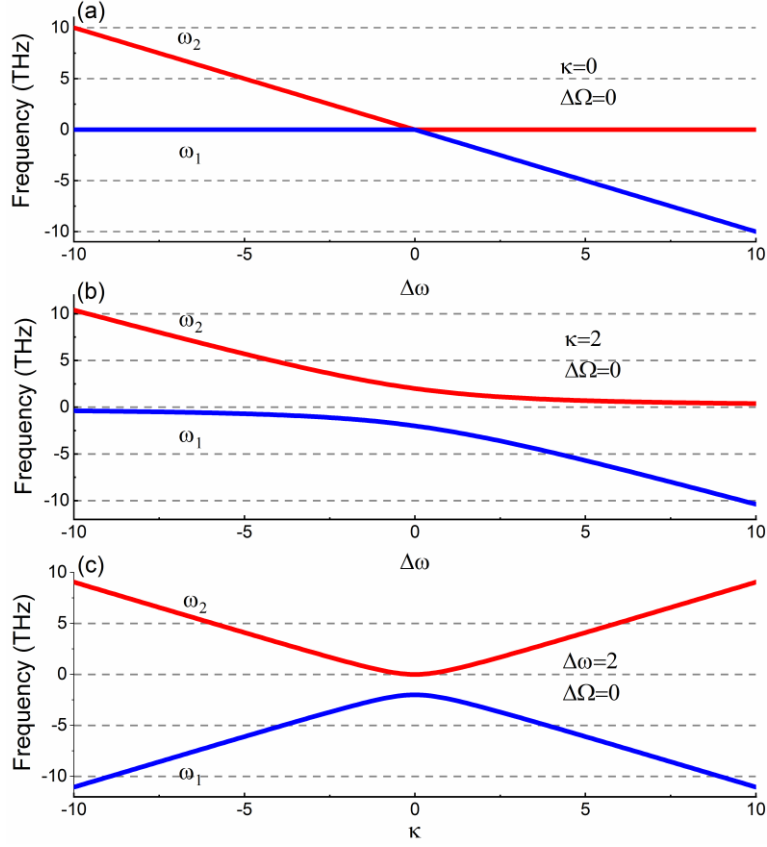


**Fig. 5** The evolution of the eigenfrequency of the coupled oscillators; **(a)** the evolution of the two eigenvalues of the coupled oscillators with the change of the resonant frequency difference of the two oscillators for the case  $\Delta\Omega = \kappa = 0$  ; **(b)** the symmetrical anti-cross evolution of the eigenfrequencies of the coupled oscillators for the case  $\Delta\Omega = 0$  and  $\kappa \neq 0$  ; **(c)** the symmetric evolution of the eigenfrequencies of the coupled oscillators for the case  $\Delta\omega \neq 0$  .

## (2) Plasmonic coupling model

We first briefly review the model description in literature[28, 29]. In the near-field, the interaction between metal structures is dominated by electrostatic fields on the nanoscale[26, 28, 29]. According to the analysis of the previous numerical calculation results, it is considered that the bright mode near the dark mode is a detectable plasmon. The electric potential solution of the Poisson equation for the all charges can be written as

$$\varphi(x) = \int \frac{\rho_e(x')}{4\pi\epsilon_0 |x-x'|} e^{-|x-x'|/l_s} dV' \quad (3)$$

Where  $l_s$  is called the shielding  $l_s^2 = \frac{\varepsilon_0 kT}{e^2 \sigma_{e0}}$ ,  $|\mathbf{x} - \mathbf{x}'|$  is the distance of the interaction between bright and dark modes. In the case of near-field action,  $|\mathbf{x} - \mathbf{x}'|$  satisfies the relationship  $|\mathbf{x} - \mathbf{x}'| = l_s$ ; therefore, the exponential term can be expanded with series and retained to the first three terms, for example  $Exp\left(-\frac{|\mathbf{x} - \mathbf{x}'|}{l_s}\right) \approx 1 - \frac{|\mathbf{x} - \mathbf{x}'|}{l_s} + \frac{1}{2}\left(\frac{|\mathbf{x} - \mathbf{x}'|}{l_s}\right)^2$ . Assuming that the charge density is only concentrated in a small volume range  $\Delta V$ , then  $\rho_e(x')\Delta V = Q$ . From this, the electric potential can be expressed as:

$$\varphi(x) = \varphi_0 + \frac{Q}{4\pi\varepsilon_0} \left( \frac{1}{|\mathbf{x} - \mathbf{x}'|} - \frac{1}{l_s} \right) + \frac{Q}{8\pi\varepsilon_0 l_s^2} |\mathbf{x} - \mathbf{x}'| \quad (4)$$

The first three terms are the initial potential, the Coulomb potential, and the electrostatic potential, respectively. The potential energy can be expressed as  $\Delta W = \frac{1}{2} Q \varphi(x) = \frac{1}{2} Q \left( \varphi_0 + \frac{Q}{4\pi\varepsilon_0} \left( \frac{1}{|\mathbf{x} - \mathbf{x}'|} - \frac{1}{l_s} \right) + \frac{Q}{8\pi\varepsilon_0 l_s^2} |\mathbf{x} - \mathbf{x}'| \right)$ . Meanwhile, the absorption energy of plasmonic the bright mode is  $\Delta W = N\hbar\Omega$ , where  $N$  is the number of nanoplasmons,  $\Omega$  is the resonant frequency of the plasmons. When the potential energy and the absorption energy are equal, the resonance frequency of the bright mode can be obtained as

$$\begin{aligned} \Omega_i &= \Omega^0 + \frac{Q^2}{8\pi\varepsilon_0 N\hbar} \left( \frac{1}{|\mathbf{x} - \mathbf{x}'|} - \frac{1}{l_s} \right) + \frac{Q^2}{16\pi\varepsilon_0 l_s^2 N\hbar} |\mathbf{x} - \mathbf{x}'| \\ &= \left( \Omega^0 - \frac{Q^2}{8\pi\varepsilon_0 l_s N\hbar} \right) + \frac{Q^2}{8\pi\varepsilon_0 N\hbar} \left( \frac{1}{|\mathbf{x} - \mathbf{x}'|} \right) + \frac{Q^2}{16\pi\varepsilon_0 l_s^2 N\hbar} |\mathbf{x} - \mathbf{x}'| \\ &= \Omega^{i0} + \frac{d_{i1}}{|\mathbf{x} - \mathbf{x}'|} + d_{i2} |\mathbf{x} - \mathbf{x}'| \end{aligned} \quad (5)$$

The symbols  $i = 1, 2$  represent the two modes after the splitting of the bright mode;  $|\mathbf{x} - \mathbf{x}'|$  is the center distance of the coupling between the nanoring and the nanorod;  $\Omega^{i0}$  (THz) is the constant term and determines the initial frequency;  $d_{i1}$  (THz/nm) is Coulomb potential coefficient;  $d_{i2}$  (THz/nm) is electrostatic potential coefficient. Eq. (5) describes that the

frequency of the bright mode of the coupled plasmon is equal to the real part of the eigenfrequency obtained by the coupling model of the harmonic oscillator from Eq. (2), i.e.,  $\Omega_{1,2} = \omega_{1,2}^0$ . The relationship between the coupling parameter of plasmons and the interaction distance can be written as

$$\begin{aligned}\omega_{1,2} &= \Omega^{i0} + \frac{d_{i1}}{|\mathbf{x} - \mathbf{x}'|} + d_{i2} |\mathbf{x} - \mathbf{x}'| \\ &= \Delta\Omega - \frac{\Delta\omega}{2} m \sqrt{\kappa^2 + \left(\frac{\Delta\omega}{2}\right)^2}\end{aligned}\quad (6)$$

## 5. Results discussion

According to the previous numerical calculation results and electric field distribution diagram, the interaction distance between nanoring plasmons and nanorod plasmons is expressed as the distance from the center of the nanoring to the center of the nanorod, as shown in Fig. 6 (a, b). In this way, the coupling distance can be expressed as  $|\mathbf{x} - \mathbf{x}'| = \sqrt{x^2 + y^2}$ . When the length of the nanorods changes,  $x$  is a variable and  $y$  is a constant; when the gap between the nanorod and the nanoring changes,  $y$  is a variable and  $x$  is a constant. When the nanorods revolve around the center of the nanorods, the expression  $|\mathbf{x} - \mathbf{x}'| = \sqrt{x^2 + y^2}$  remains unchanged.

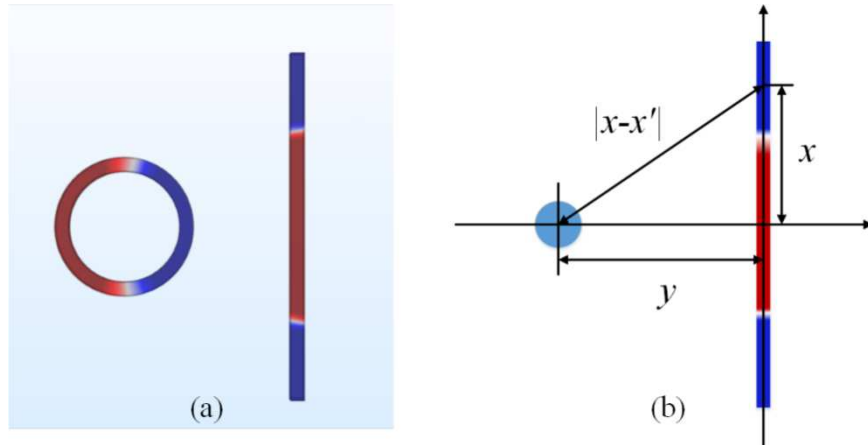


**Fig.6** (a) The schematic diagram of the electric field distribution of the the nanoring and nanorod. (b) The coupling distance of the nanoring and nanorod simplified diagram.

The numerical calculation results of anti-crossing evolution of the dimer with the Finite element method (FEM) are shown in the scattered points in Fig. 7(a). The curvature of the upper curve is greater than that of the lower curve, the two curves are asymmetric. Therefore, the result cannot be explained reasonably by the harmonic oscillator coupling model. Then according to the plasmon coupling theory model Eq. (6), we calculate the dimer resonant absorption peak with the change of the nanorod's length, as the solid line in Fig. 7(a) shown this. The asymmetry of the two curves in Fig. 7(a) is dominated by two parameters of the frequency offset  $\Delta\Omega$  and the coupling coefficient  $\kappa$ , which are function of the coupling distance. Both the Coulomb potential and electrostatic potential are important in the coupling process. In Fig. 7(b),  $(\omega_1 + \omega_2)/2$  corresponds to the evolution curve of  $\Delta\Omega - \Delta\omega/2$ , and  $(\omega_2 - \omega_1)/2$  corresponds to the evolution relationship of  $\left(\kappa^2 + \left(\frac{\Delta\omega}{2}\right)^2\right)^{1/2}$ . The two curves behave differently as the length of the nanorod changes. It shows that the parameters of the of the frequency offset  $\Delta\Omega$  and the coupling coefficient  $\kappa$  have different behave withe change of the nanorod's length.

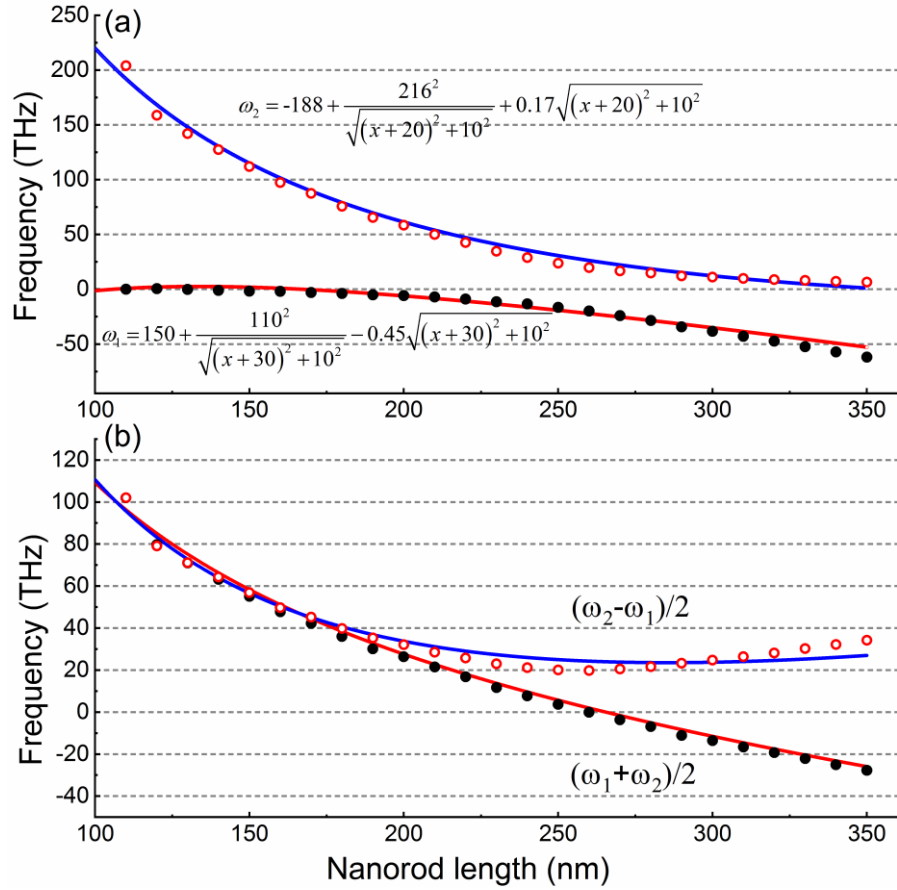


**Fig. 7** (a) The two scatter curves are the absorption peak with the change of the nanorod's length in Fig. 2, and the solid line is the calculation result of the coupling model; (b) The evolution of coupling parameters with the change of the nanorod's length. The ordinate is based on the resonance frequency of a single nanoring as the origin.

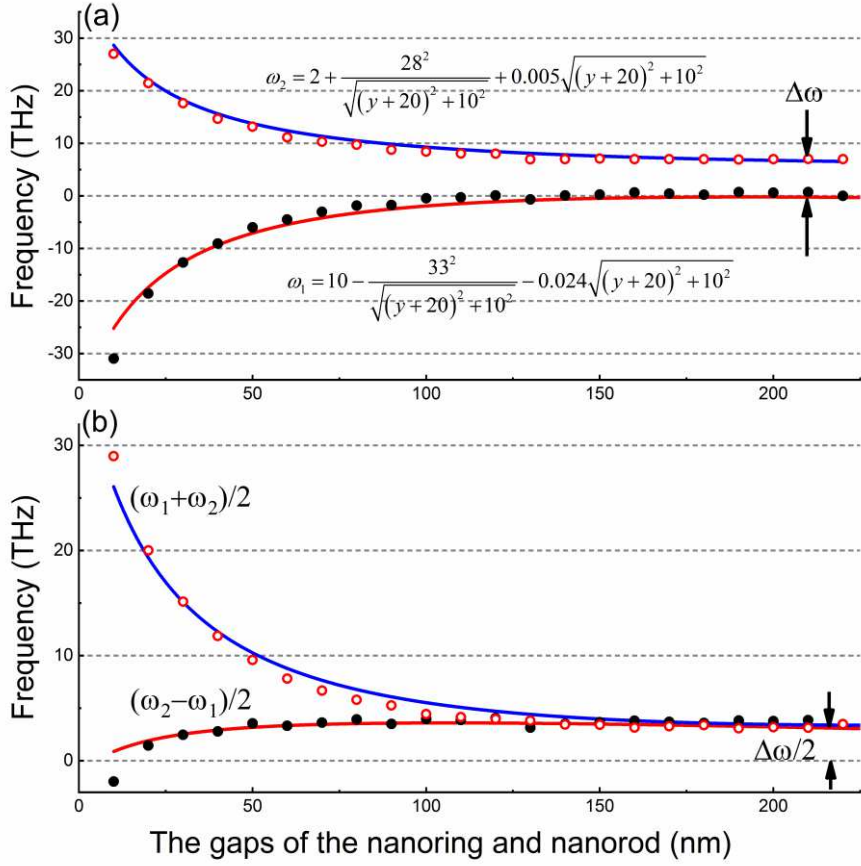


**Fig. 8 (a)** The two scatter curves are the evolution of the resonance absorption peak in Fig. 3 with the change of the distance between the nanoring and the nanorod. The solid line is the calculation result of Eq. (6); **(b)** The evolution of coupling parameters with the change of the nanorod's length. The ordinate is based on the resonance frequency of a single nanoring as the origin.

Fig. 8 shows the evolution of the splitting resonant absorption peaks of the bright mode caused by the coupling of the nanoring bright mode and the nanorod dark mode with the gap change between the nanoring and the nanorod. The solid line in Fig. 8(a) is the calculation result by using Eq. (6); the scatter curve data come from the numerical calculation in Fig. 3. When the coupling distance is larger, the coupling effect disappears. The affection of the Coulomb potential is obviously larger than that of the electrostatic potential in the coupling process. At this time, the distance between the two curves in Fig. 8(a, b) can be written as

$$\begin{cases} \omega_1 = -\frac{\Delta\omega}{2} + \frac{\Delta\omega}{2} = 0 \\ \omega_2 = \frac{\Delta\omega}{2} + \frac{\Delta\omega}{2} = \Delta\omega \end{cases} \quad (7)$$

$$\frac{\omega_1 + \omega_2}{2} = \frac{\omega_2 - \omega_1}{2} = \frac{\Delta\omega}{2}$$

Obviously, the closer the coupling distance, the greater the coupling strength, and the farther the splitting distance of the resonance absorption peak. It also shows that the two coupling parameters have different evolution laws. Moreover, under the influence of different coupling conditions, the evolution law of coupling parameters is different, as shown in Fig. 7 and Fig. 8 (b). In the above two cases, the change of the coupling condition caused by the change of the dimer structure can be attributed to the change of the coupling distance. Therefore, the previous coupling model can be used to give a good explanation. The difference is the change of coupling distance, one is longitudinal and the other is horizontal, as shown in Fig. 7 and Fig. 8.

## 6. Conclusion

In summary, we designed a dimer structure composed by a nanoring and a nanorod in the article. Using the coupling model to get the relationship between the coupling parameters and the coupling distance is the purpose of this article. The Coulomb potential and electrostatic potential interaction dominate the coupling processes. By combining the harmonic oscillator model with the coupling model, we not only explain the effect of the coupling distance change on the absorption spectra of the dimer, but also successfully explain the anti-crossing physical effect. Moreover, we discussed coupling process under three conditions. First, the plasmon of the nanoring is excited directly by the light field when the polarization direction of the excitation light field is perpendicular to the nanorod, and it is a bright mode. Meantime, the bright mode induce nanorod to generate a dark mode, then the interaction or coupling between them causes the bright mode split. At this time, the splitting bright mode exhibits the anti-crossing characteristics by changing the nanorod's length. Second, the smaller the coupling distance is, the stronger the coupling is, the larger the bright mode splitting distance is. As the coupling distance increases, the coupling becomes weaker. Finally, the change of the coupling between the bright mode and the dark mode

is observed with the change of the polarization direction of the excitation light field.

**Funding:** This research did not receive any specific grants from funding agencies.

**Availability of data and material:** The authors declare that data and material are available.

**Code availability:** The data that support the findings of this study are available from the corresponding author upon reasonable request.

**Authors' contributions:** All authors contributed to the study conception and design. COMSOL calculations and data collection and analysis were performed by Jianxin Zhang; review and editing were performed by Jian Zhang and Yongfang Li. All authors have read and agreed to the published version of the manuscript.

### **Compliance with Ethical Standards**

**Conflicts of interest:** The authors declare that they have no conflicts of interest.

### **References**

1. Harris SE (1996) Electromagnetically Induced Transparency in an Ideal Plasma. *Phys Rev Lett* 77 (27):5357.
2. Fleischhauer M, Imamoglu A, Marangos JP (2005) Electromagnetically induced transparency: Optics in coherent media. *Rev Mod Phys* 77 (2):633-673.
3. Yin X, Feng T, Yip S, Liang Z, Hui A, Ho JC, Li J (2013) Tailoring electromagnetically induced transparency for terahertz metamaterials: From diatomic to triatomic structural molecules. *Appl Phys Lett* 103 (2):021115.
4. Jing H, Zhu Z, Zhang X, Gu J, Tian Z, Ouyang C, Han J, Zhang W (2013) Plasmon-induced transparency in terahertz metamaterials. *Sci China Inf Sci* 56 (12):120406.
5. Hau LV, Harris SE, Dutton Z, Behroozi CH (1999) Light speed reduction to 17 metres per second in an ultracold atomic gas. *Nature* 397 (6720):594-598.

6. Liu X, Gu J, Singh R, Ma Y, Zhu J, Tian Z, He M, Han J, Zhang W (2012) Electromagnetically induced transparency in terahertz plasmonic metamaterials via dual excitation pathways of the dark mode. *Appl Phys Lett* 100 (13):131101.
7. Liu YC, Li BB, Xiao YF (2017) Electromagnetically induced transparency in optical microcavities. *Nanophotonics* 6 (5):789-811.
8. Xiao S, Wang T, Liu T, Yan X, Li Z, Xu C (2018) Active modulation of electromagnetically induced transparency analogue in terahertz hybrid metal-graphene metamaterials. *Carbon* 126:271-278.
9. Krauss TF (2008) Why do we need slow light? *Nature Photonics* 2 (8):448-450.
10. Kekatpure RD, Barnard ES, Cai W, Brongersma ML (2010) Phase-Coupled Plasmon-Induced Transparency. *Phys Rev Lett* 104 (24):243902.
11. Maleki L, Matsko AB, Savchenkov AA, Ilchenko VS (2004) Tunable delay line with interacting whispering-gallery-mode resonators. *Opt Lett* 29 (6):626-628.
12. Yanik MF, Suh W, Wang Z, Fan SH (2004) Stopping light in a waveguide with an all-optical analog of electromagnetically induced transparency. *Phys Rev Lett* 93 (23):233903.
13. Xu QF, Sandhu S, Povinelli ML, Shakya J, Fan SH, Lipson M (2006) Experimental realization of an on-chip all-optical analogue to electromagnetically induced transparency. *Phys Rev Lett* 96 (12):123901.
14. Tassin P, Zhang L, Koschny T, Economou EN, Soukoulis CM (2009) Low-Loss Metamaterials Based on Classical Electromagnetically Induced Transparency. *Phys Rev Lett* 102 (5):053901.
15. Liu N, Langguth L, Weiss T, Kaestel J, Fleischhauer M, Pfau T, Giessen H (2009) Plasmonic analogue of electromagnetically induced transparency at the Drude damping limit. *Nature Materials* 8 (9):758-762.
16. Zhang S, Genov DA, Wang Y, Liu M, Zhang X (2008) Plasmon-induced transparency in metamaterials. *Phys Rev Lett* 101 (4):047401.
17. Papasimakis N, Fedotov VA, Zheludev NI, Prosvirnin SL (2008) Metamaterial Analog of Electromagnetically Induced Transparency. *Phys Rev Lett* 101 (25):253903.
18. Alzar CLG, Martinez MAG, Nussenzveig P (2002) Classical analog of electromagnetically induced transparency. *Am J Phys* 70 (1):37-41.
19. Novotny L (2010) Strong coupling, energy splitting, and level crossings: A classical perspective. *Am J Phys* 78 (11):1199-1202.
20. Lovera A, Gallinet B, Nordlander P, Martin OJF (2013) Mechanisms of Fano Resonances in Coupled Plasmonic Systems. *Acs Nano* 7 (5):4527-4536.
21. Cheng H, Chen S, Yu P, Duan X, Xie B, Tian J (2013) Dynamically tunable plasmonically induced

- transparency in periodically patterned graphene nanostrips. *Appl Phys Lett* 103 (20):.
22. Zhang J, Xu Y, Zhang J, Ma P, Zhang M, Li Y (2018) Extended coupled Lorentz oscillator model and analogue of electromagnetically induced transparency in coupled plasmonic structures. *Journal of the Optical Society of America B-Optical Physics* 35 (8):1854-1860.
  23. Ma PP, Zhang J, Liu HH, Zhang J, Xu YG, Wang J, Zhang MQ, Li YF (2016) Plasmon induced transparency in the trimer of gold nanorods. *Acta Physica Sinica* 65 (21):203112.
  24. Zuloaga J, Nordlander P (2011) On the Energy Shift between Near-Field and Far-Field Peak Intensities in Localized Plasmon Systems. *Nano Letters* 11 (3):1280-1283.
  25. Lassiter JB, Sobhani H, Knight MW, Mielczarek WS, Nordlander P, Halas NJ (2012) Designing and Deconstructing the Fano Lineshape in Plasmonic Nanoclusters. *Nano Letters* 12 (2):1058-1062.
  26. Davis TJ, Gomez DE (2017) Colloquium: An algebraic model of localized surface plasmons and their interactions. *Rev Mod Phys* 89 (1):011003.
  27. Johnson PB, Christy RW (1972) Optical Constants of the Noble Metals. *Physical Review B* 6 (12):4370-4379.
  28. Zhang J, Xu YG, Zhang JX, Guan LL, Li YF (2020) Bright-Dark Mode Coupling Model of Plasmons. *Chinese Physics Letters* 37 (3):037101.
  29. Guan L, Zhang J, Xu Y, Zhang J, Li Y (2019) Impact of the Coulomb Potential and the Electrostatic Potential on the Eigen-Frequencies of the Coupled Plasmons. *Plasmonics* 15 (2):351-359.

# Figures

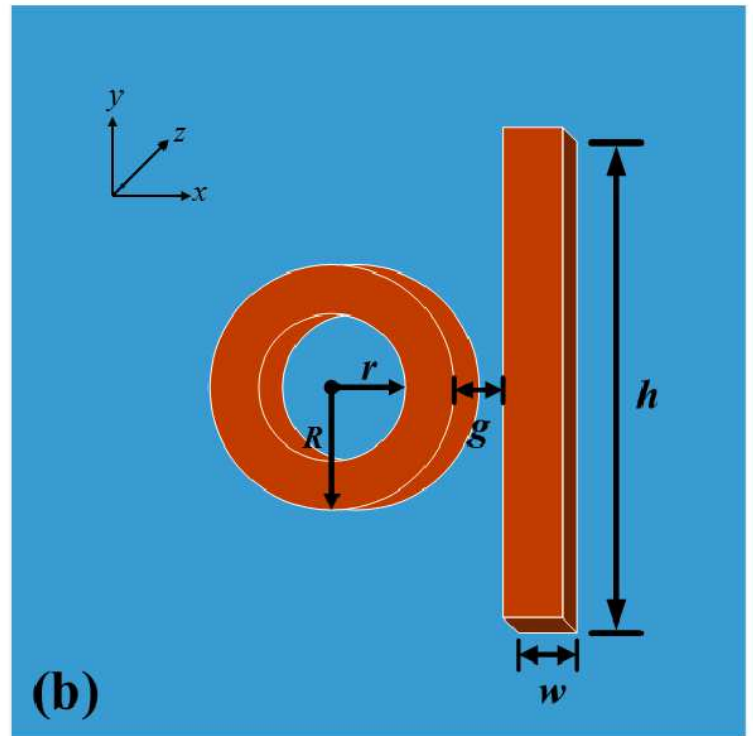
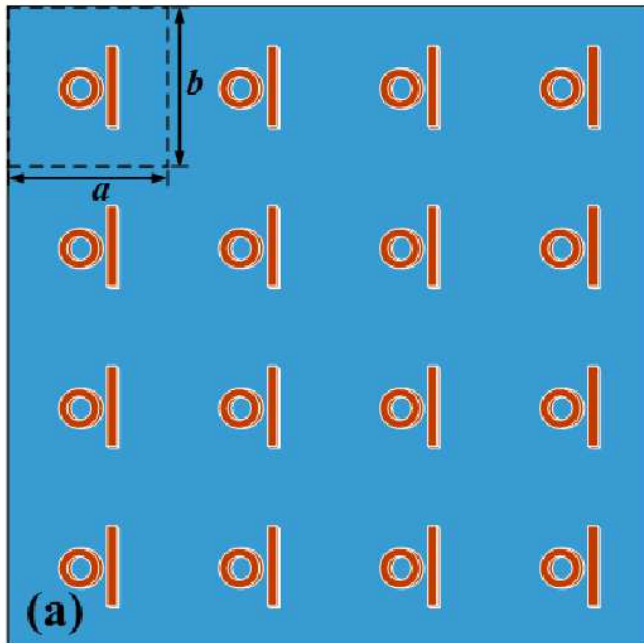
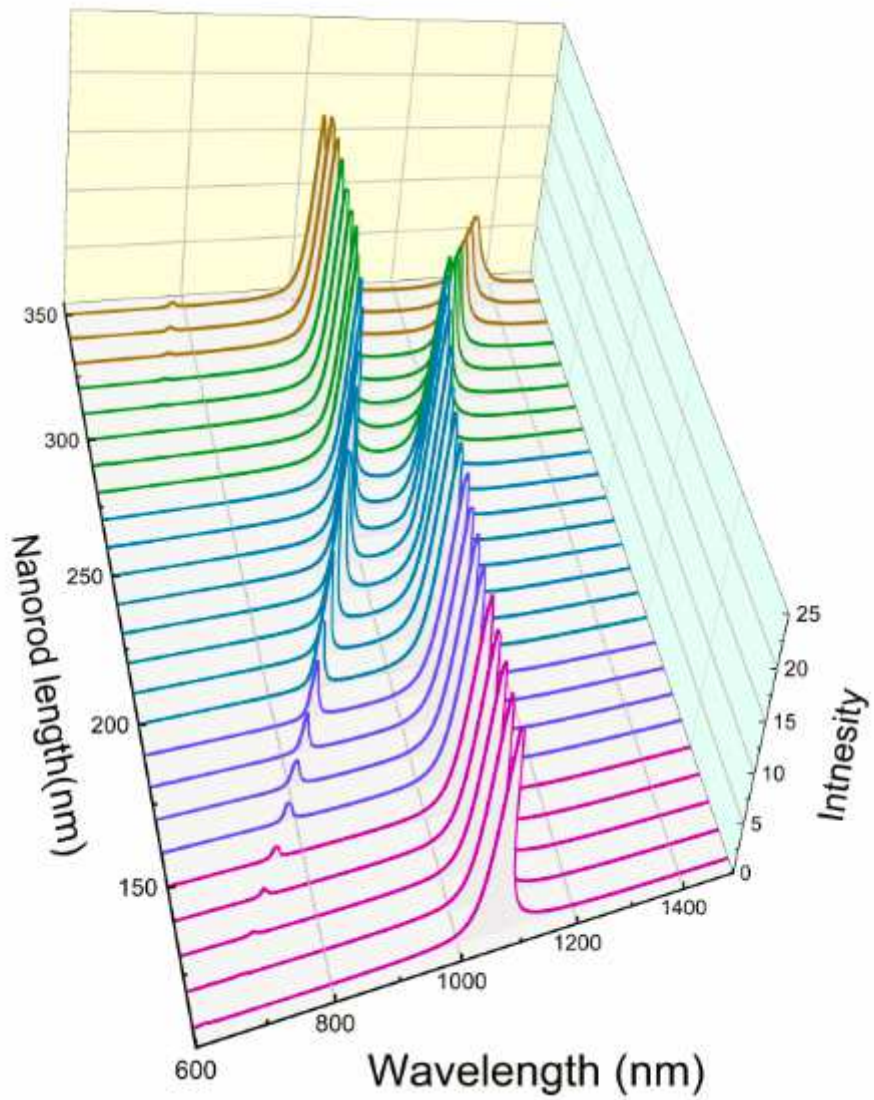


Figure 1

Schematic diagram of the nanoring-nanorod dimer structure. (a) Periodically arranged dimer units. (b) Specific structure of a dimer unit.



**Figure 2**

The evolution of the two resonant absorption spectra of the nanoring with the length of the nanorods in the dimer. This is an anti-crossing characteristic. The distance between the two is kept at  $g = 20$  nm.

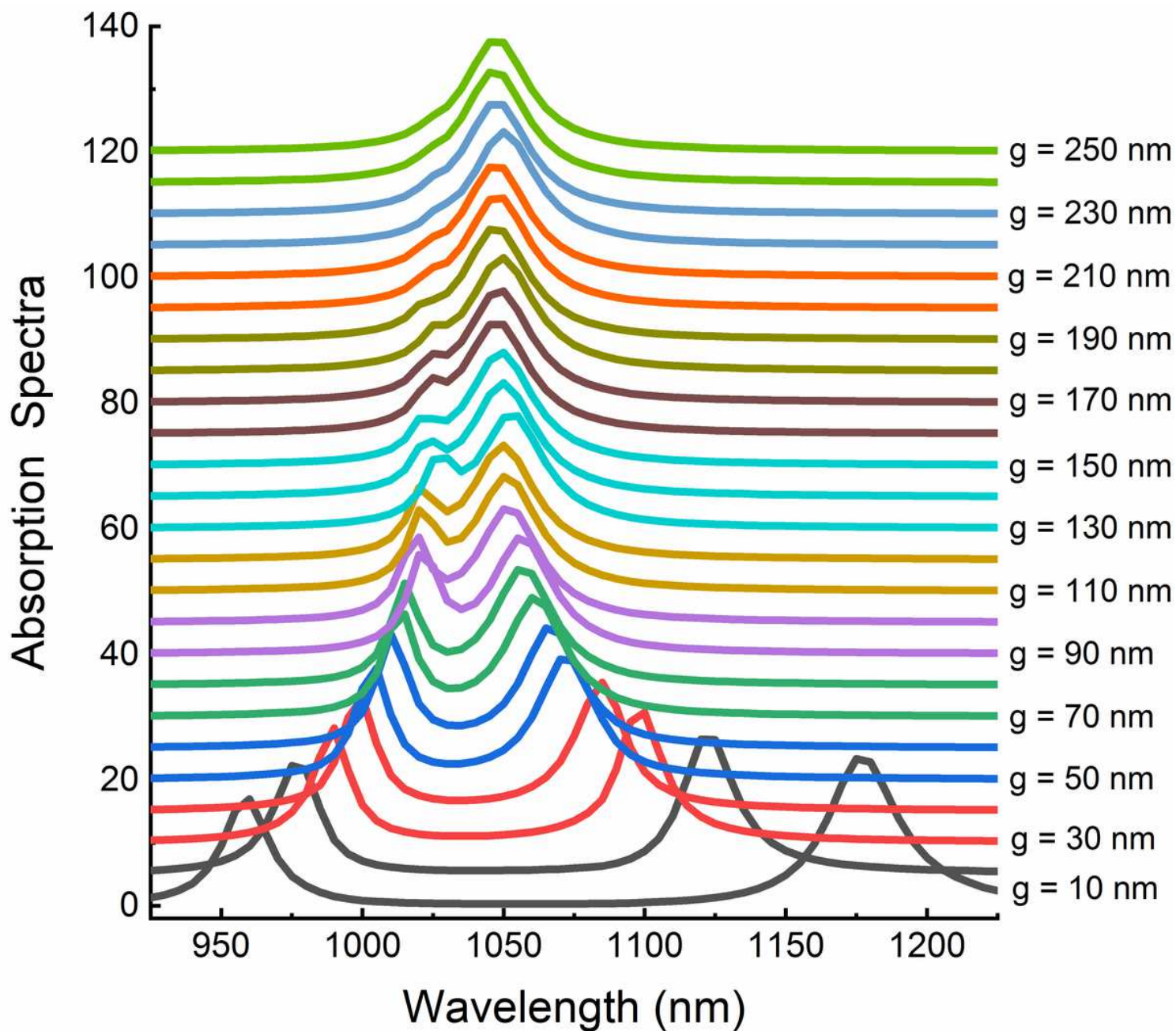
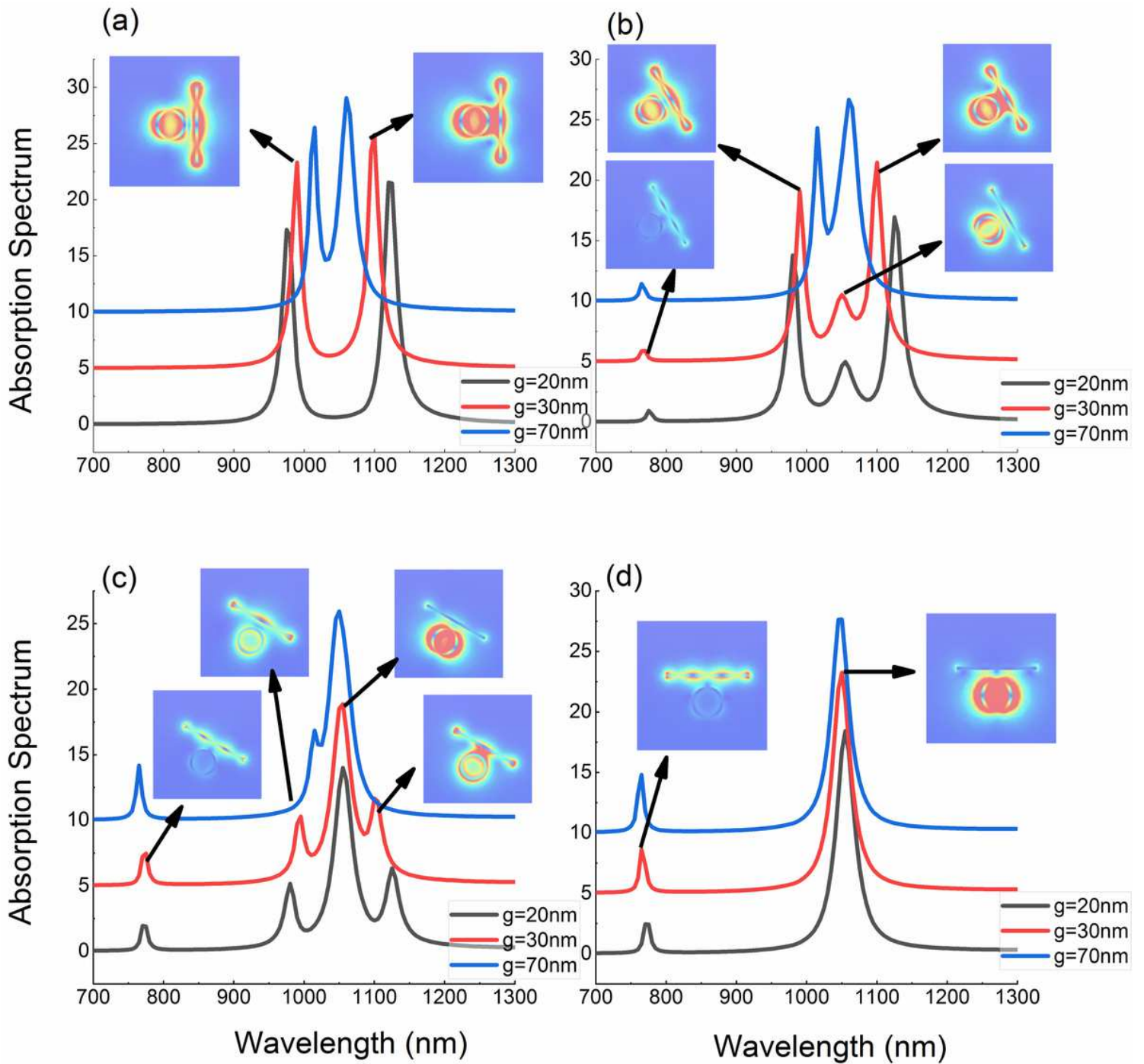


Figure 3

The evolution of the two resonant absorption spectra of nanorings with the change of the gaps between nanorod and nanoring in the dimer. The length of the nanorod is  $L = 250$  nm.



**Figure 4**

The evolution of the absorption spectra with the change of the angles between the polarization direction of the excitation light and the nanorod, which are  $90^\circ$ ,  $60^\circ$ ,  $30^\circ$ , and  $0^\circ$ , respectively.

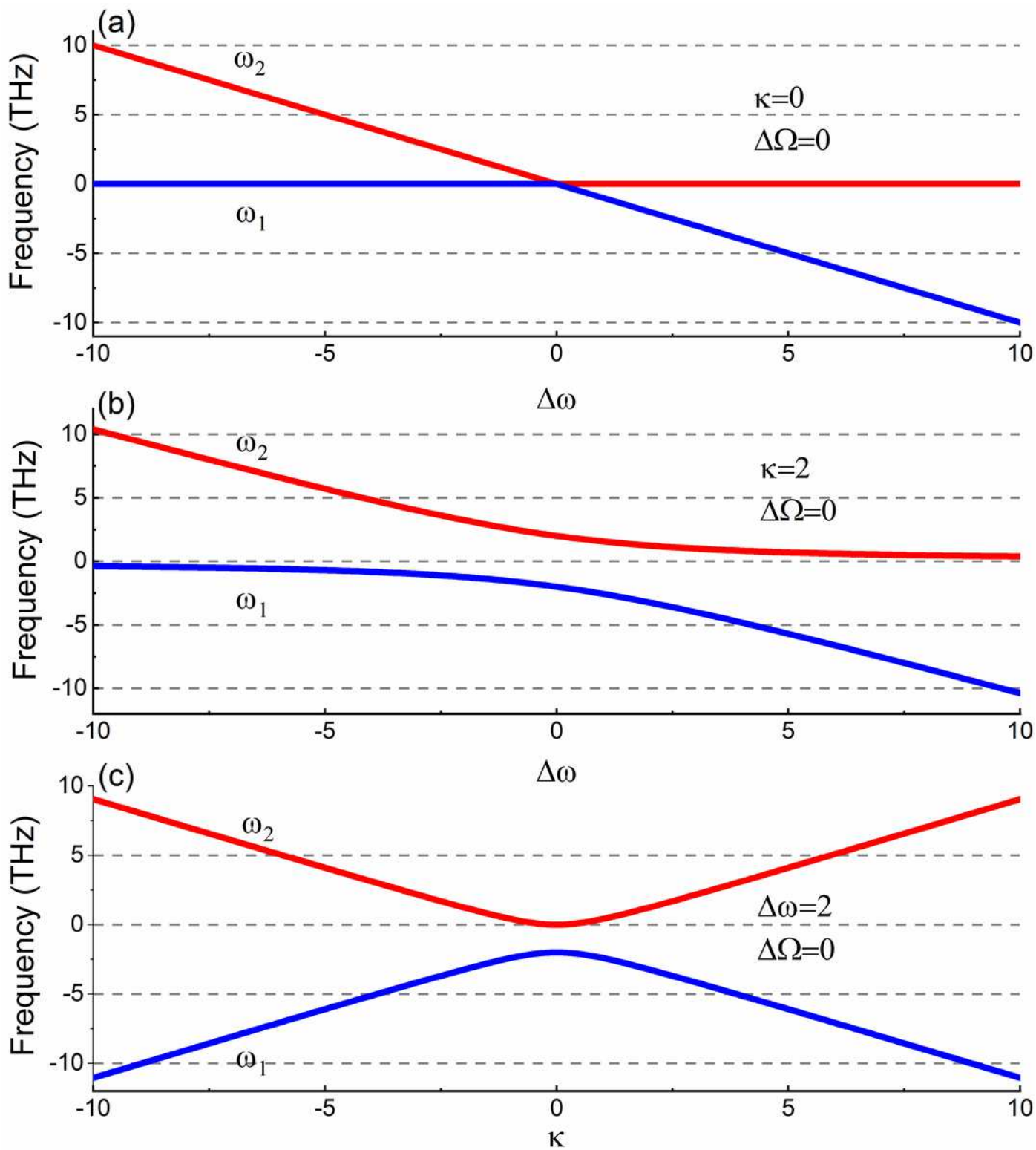
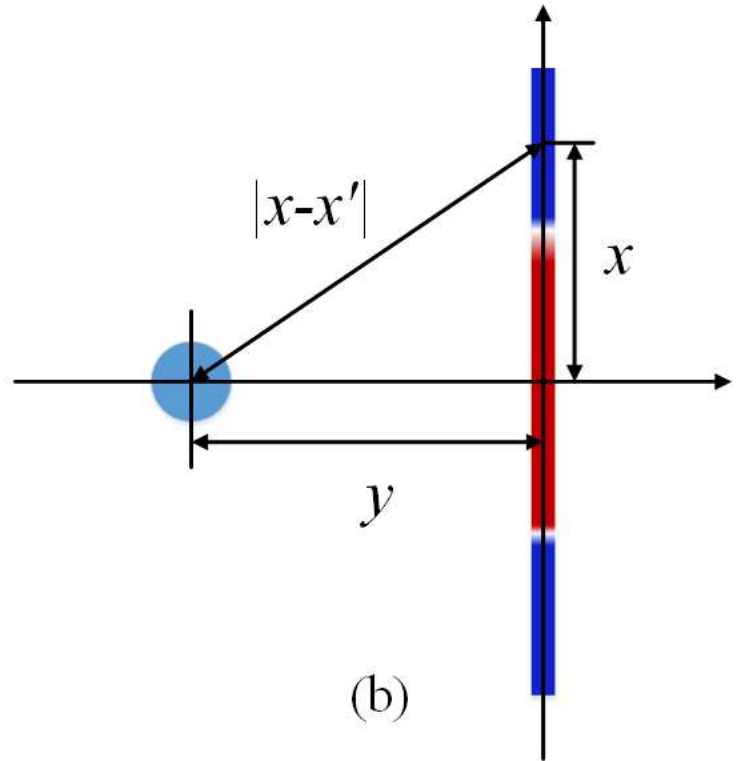
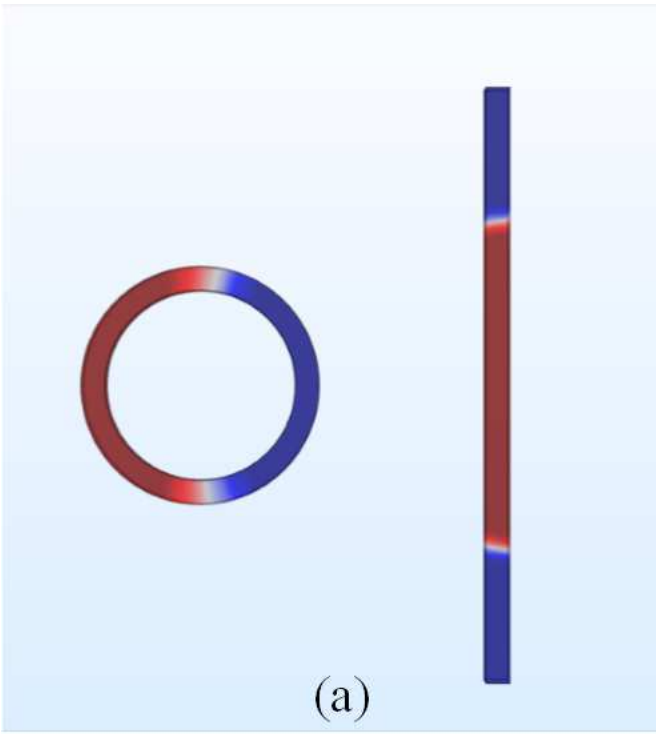


Figure 5

"See the Supplemental Files section for the complete figure caption".



**Figure 6**

(a) The schematic diagram of the electric field distribution of the the nanoring and nanorod. (b) The coupling distance of the nanoring and nanorod simplified diagram.

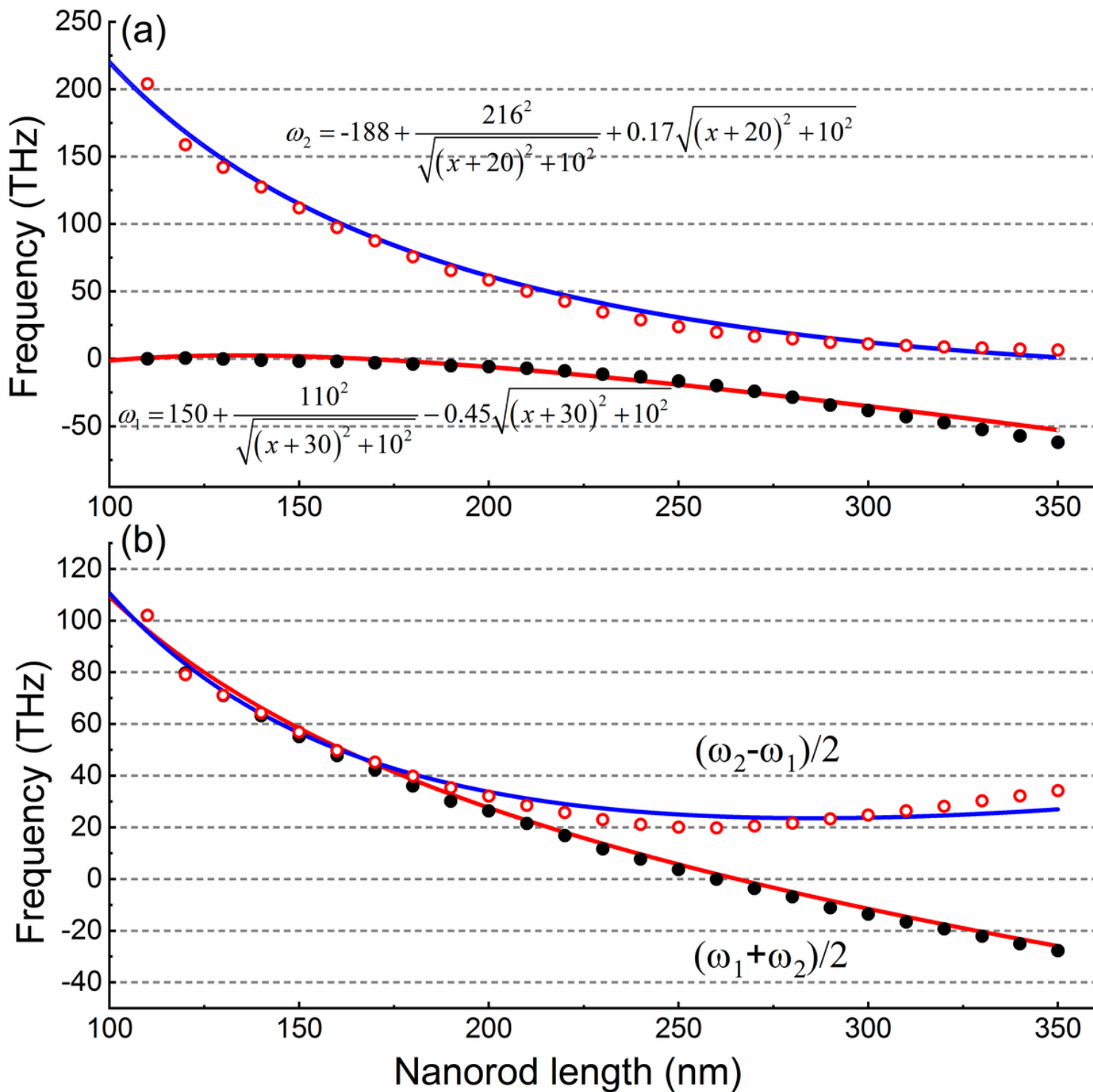


Figure 7

(a) The two scatter curves are the absorption peak with the change of the nanorod's length in Fig. 2, and the solid line is the calculation result of the coupling model; (b) The evolution of coupling parameters with the change of the nanorod's length. The ordinate is based on the resonance frequency of a single nanoring as the origin.

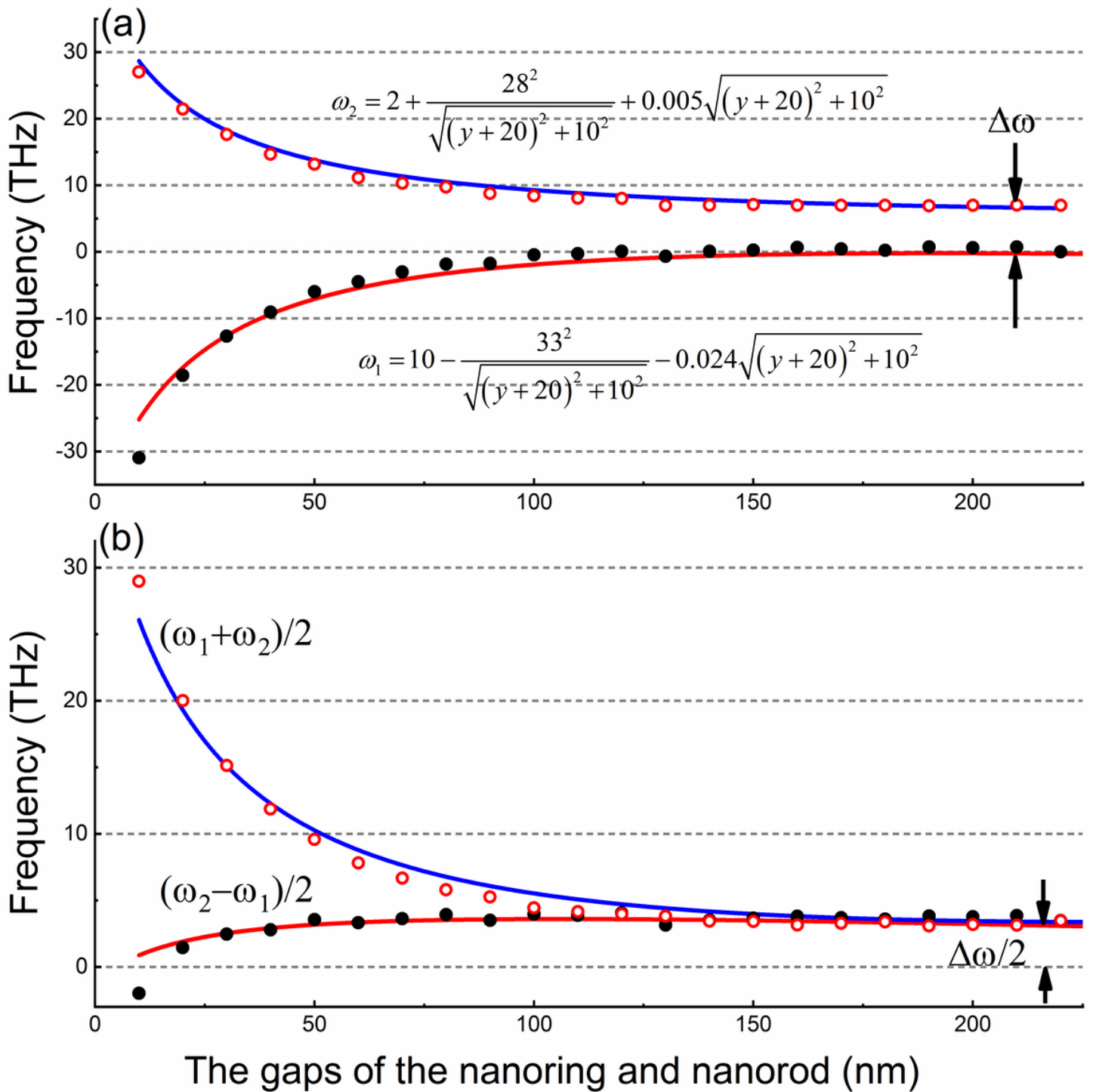


Figure 8

(a) The two scatter curves are the evolution of the resonance absorption peak in Fig. 3 with the change of the distance between the nanoring and the nanorod. The solid line is the calculation result of Eq. (6); (b) The evolution of coupling parameters with the change of the nanorod's length. The ordinate is based on the resonance frequency of a single nanoring as the origin.

## Supplementary Files

This is a list of supplementary files associated with this preprint. Click to download.

- [FigCaption5.docx](#)